Tracking and Behavior Reasoning of Moving Vehicles Based on Roadway Geometry Constraints

Kichun Jo, *Member, IEEE*, Minchul Lee, *Student Member, IEEE*, Junsoo Kim, *Member, IEEE*, and Myoungho Sunwoo, *Member, IEEE*

***Abstract*—Tracking and behavior reasoning of surrounding vehicles on a roadway are keys for the development of automated vehicles and an advanced driver assistance system (ADAS). Based on dynamic information of the surrounding vehicles from the tracking algorithm and driver intentions from the behavior reasoning algorithm, the automated vehicles and ADAS can predict possible collisions and generate safe motion to avoid accidents. This paper presents a unified vehicle tracking and behavior reasoning algorithm that can simultaneously estimate the vehicle dynamic state and driver intentions. The multiple model filter based on various behavior models was used to classify the vehicle behavior and estimate the dynamic state of surrounding vehicles. In addition, roadway geometry constraints were applied to the unified vehicle tracking and behavior reasoning algorithm in order to improve the dynamic state estimation and the behavior classification performance. The curvilinear coordinate system was constructed based on the precise map information in order to apply the roadway geometry to the tracking and behavior reasoning algorithm. The proposed algorithm was verified and evaluated through experiments under various test scenarios. From the experimental results, we concluded that the presented tracking and behavior reasoning algorithm based on the roadway geometry constraints provides sufficient accuracy and reliability for automated vehicles and ADAS applications.**

***Index Terms*—Behavior reasoning, curvilinear coordinate, geometry constraints, interacting multiple model (IMM) filter, roadway map, vehicle tracking.**

I. Introduction

AUTOMATED vehicle and advanced driver assistance system (ADAS) are the most promising solution to reduce traffic accidents on roadways. The system can prevent accidents by generating safe motion and assisting vehicle control. To generate safe motion of the vehicle on roadways, understanding of the dynamic features of surrounding vehicles is particularly important because the safety margin for surrounding moving vehicles can be calculated by predicting their motions and behaviors. To accurately predict vehicle motions and behaviors, the current dynamic state and behavior of the moving vehicle should be accurately estimated using two functions: vehicle motion tracking and behavior reasoning. The vehicle motion tracking algorithm estimates the dynamic state of vehicle motion based on Bayesian filtering approaches and the behavior reasoning algorithm detects the intention of the surrounding vehicles based on the tracking results.

There are many previous studies concerning the tracking of moving vehicles on roadways. The tracking systems normally use on-board sensors, such as cameras [1]–[6], LIDARs [7]–[9], and radar [10]–[13] for vehicle detection. In addition to individual sensor-based tracking, there have been many studies of the information fusion of multiple sensors to improve the accuracy and reliability of the vehicle tracking algorithm [14]–[18]. Many types of Bayesian filters such as a Kalman filter, extended Kalman filter, unscented Kalman filter, multiple model filter, and particle filter are usually applied for the tracking algorithm. However, these algorithms, which depend only on on-board sensors, possess performance constraints because of the sensor limitations such as a short detection range, narrow field of view, signal noise, and unexpected occupied obstacles. In order to overcome the tracking constraints based on on-board sensors, we applied the roadway geometry information to the tracking algorithm. The roadway geometry information from the digital map can constrain the motion of moving vehicles. Therefore, it is possible to reduce the detection sensor noise and improve the reliability and accuracy of the tracking algorithm.

Behavior reasoning algorithms for classifying the intention of surrounding vehicles are also widely studied for automated driving and ADAS applications in order to avoid traffic accidents [19]–[22]. Machine learning algorithms such as the Bayes classifier, decision tree, and support vector machine are used to infer the driver intentions on roadways [20], [21]. The vehicle motion characteristics such as the acceleration, velocity, and distance gap can be applied as criteria to classify the target vehicle behavior [23], [24]. Wireless communication can directly access the behavior information of surrounding vehicles [25], [26]. The probabilistic drivability based on the discrete sample space can predict the safety level of moving vehicles to prevent collisions [27]–[29]. The Bayesian network is used to recognize the intention and safety of moving vehicles [30], [31]. In previous studies [30], [32], a unified framework for tracking

Manuscript received August 12, 2015; revised January 26, 2016, April 7, 2016, and July 11, 2016; accepted August 10, 2016. Date of publication September 23, 2016; date of current version February 1, 2017. This work was supported by the National Research Foundation of Korea grant funded by the Korean Government (Ministry of Education, Science and Technology) under Grant 2011-0017495, by the Practical Development of Wireless Low-Floor Tram under Grant 15RTRP-B067379-03 project funded by Korean Ministry of Land, Infrastructure and Transport, and the BK21 plus program under Grant 22A20130000045 under the Ministry of Education, Republic of Korea. The Associate Editor for this paper was Z. Duric.

K. Jo is with Valeo, 93012 Paris, France (e-mail: kichun.jo@valeo.com).

M. Lee and M. Sunwoo are with the Automotive Control and Electronics Laboratory (ACE Lab), Department of Automotive Engineering, Hanyang University, Seoul 133-791, South Korea.

J. Kim is with the ADAS Strategy Team, Hyundai Motor Company, Seoul 06797, South Korea.

Color versions of one or more of the figures in this paper are available online at http://ieeexplore.ieee.org.

Digital Object Identifier 10.1109/TITS.2016.2605163

and behavior reasoning was introduced for highway driving, but the algorithms did not consider the transient motion of lane changing. Furthermore, many previous studies did not precisely consider roadway geometry information from a high accuracy digital map. The precise roadway geometry information can improve the performance of the behavior reasoning algorithms.

This paper presents a unified framework for motion tracking and behavior reasoning of moving vehicles located near the ego vehicle based on roadway geometry constraints. Heterogeneous sensors such as cameras, radars, and LIDARs are used for measurements in the algorithm. The roadway geometry information is extracted from the prepared digital map. Based on the roadway geometry information, a curvilinear coordinate system is constructed which consists of longitudinal and lateral curve axes. There are many benefits for the curvilinear coordinate-based tracking and behavior reasoning from the aspects of tracking filter design and behavior classification. A multiple model filter approach is the basis of the unified framework in order to simultaneously track the vehicle motion and infer the behavior. The proposed unified tracking and behavior reasoning algorithm was intensively evaluated through utilization in various scenarios.

The main contribution of the paper can be described as three key sentences:

1) Proposition of unified (simultaneous) tracking and behavior reasoning of moving vehicles.
2) Applying the roadway geometry constraint to unified tracking and behavior reasoning.
3) Design of four vehicle motion models for multiple model filtering.

This paper is organized as follows. Section II presents the overall structure of the proposed algorithm. Section III presents the measurement vector generation method using heterogeneous vehicle detection sensors. Section IV describes the curvilinear coordinate conversion algorithm and Section V covers the unified tracking and behavior reasoning algorithm. Section VI provides verification results based on the experiences and the final section provides conclusions.

II. System Architecture

A. Overall Structure of the Algorithm

The overall structure of the unified motion tracking and behavior reasoning algorithm for moving vehicles consists of three steps: generation of the measurement list, curvilinear coordinate conversion, and unified tracking and behavior reasoning, as shown in Fig. 1.

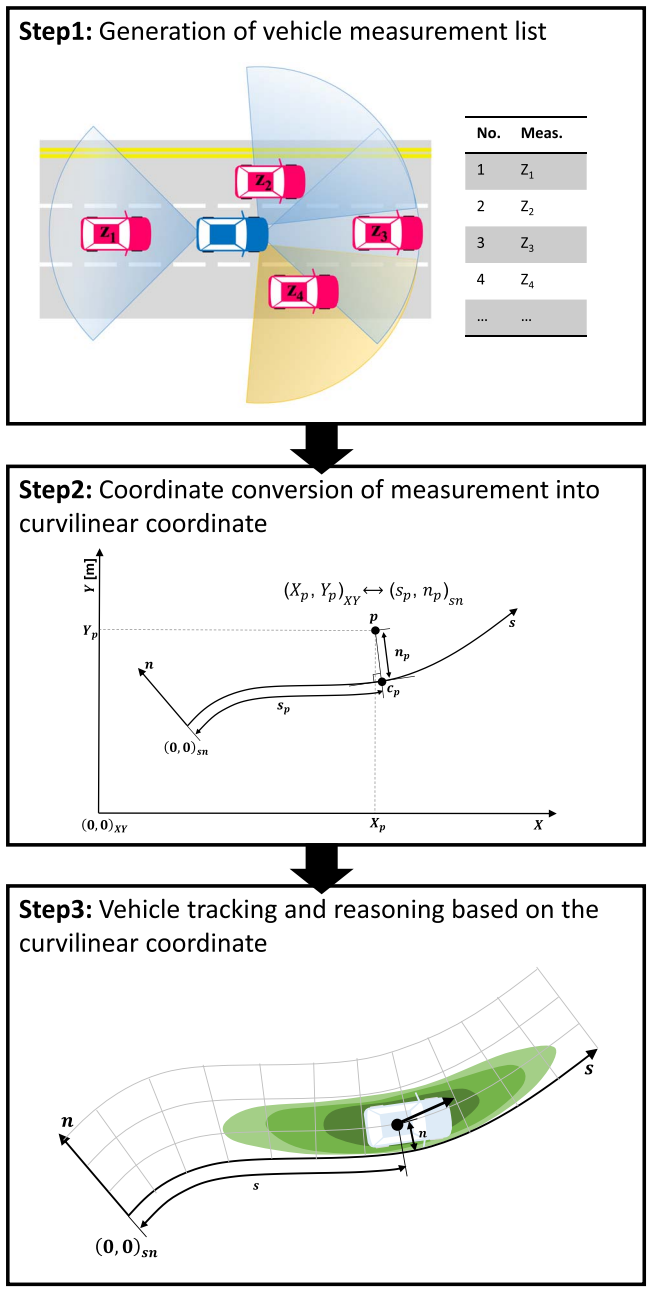

Fig. 1. Overview of the system architecture for the unified vehicle tracking and behavior reasoning algorithm.

1) Generation of the Measurement List for Moving Vehicles: Heterogeneous sensors such as LIDARs, radars, and cameras are used for the detection of moving vehicles that are located around the ego vehicle. These types of sensors normally provide the track information (such as the position, velocity, acceleration, and heading) and classification information (such as vehicle, pedestrian, and static obstacles). The track information from heterogeneous sensors may have different data formats. Therefore, the information should be rearranged into a consistent measurement vector for the unified motion tracking and behavior reasoning algorithm. In addition, the vehicle detection measurements which are not classified as the moving vehicles (zero velocity and not classified as vehicles) have to be filtered out from the measurement list because the proposed algorithm is only for tracking and behavior reasoning of the moving vehicles surrounding the ego-vehicle.

2) Curvilinear Coordinate Conversion: The roadway geometry can be extracted from the roadway geometry map. The curvilinear coordinates can be set up using the roadway geometry information where the target vehicles are located. The vehicle detection measurements which are represented in Cartesian coordinates are converted into curvilinear coordinates in order to apply the roadway geometry constraints to the tracking and reasoning algorithm.

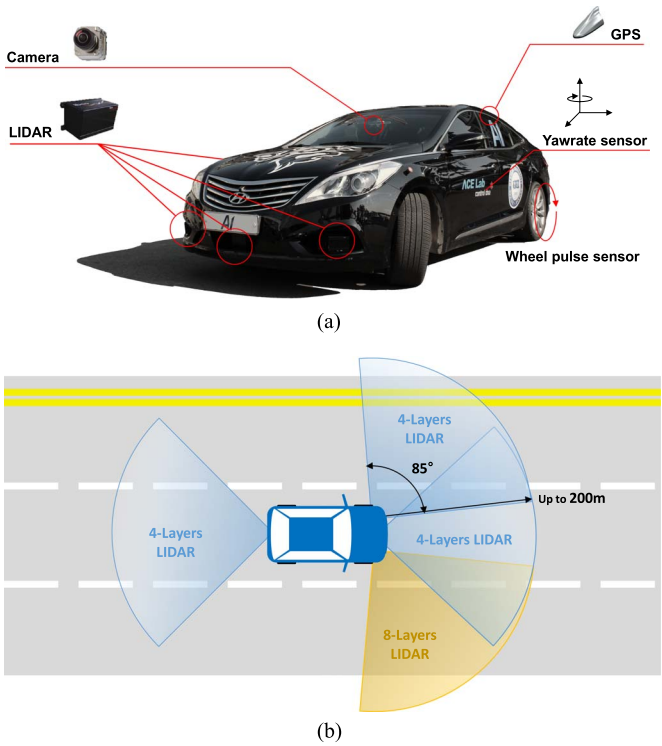

Fig. 2. Sensor configuration and ROI of LIDARs used to evaluate the unified tracking and behavior reasoning algorithm.

B. Unified Tracking and Behavior Reasoning

Unified tracking and behavior reasoning is performed based on the curvilinear coordinates. A multiple model-set is designed for representing the various motions of moving vehicles. Based on the multiple model set, an interacting multiple model (IMM) filter is applied to the unified tracking and behavior reasoning algorithm. The IMM filter simultaneously estimates the vehicle motion and infers the behavior of the moving vehicle based on a probabilistic approach.

C. Sensor Configuration

A test vehicle [Fig. 2(a)] equipped with LIDARs and a localization system was used to evaluate the unified motion tracking and behavior reasoning algorithm. Three 4-layers LIDARs are installed on the center of the front bumper, the left of the front bumper, and the center of the rear bumper, respectively. One 8-layers LIDAR is installed on the right of the front bumper in order to detect a curb more clearly. The region of interest (ROI) of covered by each LIDAR is shown in Fig. 2(b). Each LIDAR provides individual track information such as state and covariance of vehicle motion (position, velocity, and heading) in the vehicle body coordinate system and the object classification information (vehicle, pedestrian, bike, and unknown). Since the LIDAR provides a hardware synchronization protocol to synchronize with other LIDARs, we do not need to be concerned with the synchronization problem of tracking.

The localization system is an important component to extract the proper roadway geometry from the map database. In this experiment, a precise localization system (accuracy < 0.3 m) based on the integration of LIDARs, cameras, vehicle motion sensors, and GPS was used to estimate the position and heading of the ego vehicle [33], [34].

D. Roadway Map Database

The roadway geometry used in this experiment is described based on a B-spline model. The roadway map generation algorithm previously presented [35] was applied to the B-spline roadway map generation. The map generation algorithm is composed of three steps: data acquisition, sensor data fusion, and road modeling. At the data acquisition step, a probe vehicle equipped with a positioning system (such as GPS and vehicle motion sensors) obtains raw measurements for the roadway map generation. The sensor fusion algorithm based on the optimal smoothing is applied to improve the accuracy and reliability of the road geometry measurements. Based on the processed data, the iterative curve modeling algorithm (gradual correction method) generates a B-spline road geometry model with a reduced amount of control parameters.

III. Generation of the Vehicle Measurement List

Vehicles moving around the ego vehicle can be detected and traced using various types of sensors such as LIDARs, radar, and cameras. These tracking sensors usually provide the track state (position, velocity, acceleration, or heading) and classification information (vehicles, pedestrians, or static obstacles). The track and classification information of the heterogeneous sensors may have different data formats, noise characteristics, and sampling times. Therefore, we should consider the different features of the heterogeneous sensor for application to the unified motion tracking and behavior reasoning algorithm.

The different data formats of the heterogeneous sensors should be unified into a consistent measurement vector format. For instance, one sensor may provide the vehicle motion using the velocity vector in Cartesian coordinates (v_x, v_y), but another sensor may offer the speed, v, and heading, ψ, in polar coordinates. In this case, we should unify the different data formats into one consistent format. Furthermore, it is possible to filter out undesired objects (such as static objects and objects outside of the ROI) from the measurement list when the consistent measurement vector is constructed.

Accuracy and noise features of the heterogeneous vehicle detection sensors can be different depending on the detection principle, installed location, and driving environments. For example, the camera-based detection sensor can make better estimates for the side-to-side (lateral) distance of the target vehicles because it calculates the distance based on the image pixel coordinate. Also, it has superior performance for classifying the vehicle type compared to LIDARs and radar. However, since the longitudinal distance from the ego-vehicle to target vehicle is hard to estimate based on the image coordinates, the accuracy of longitudinal distance is poorer than those of radar and LIDARs. The LIDARs can provide very accurate measurements of detected vehicles, but they are impossible to use in bad weather environments (heavy rain, fog, and snow). In contrast, radar is robust in bad weather conditions, but the tracking accuracy is usually lower than that of LIDARs and it suffers from false-positive detection of unexpected metal

objects. To reflect the characteristics of each sensor in the tracking and reasoning algorithms, the performance and noise features of the sensors should be analyzed and verified before the filtering algorithm design. Then, we can apply the results of the sensor analysis to design the measurement covariance matrix for the Bayesian filter update.

Since the vehicle measurement is coming from the detection sensors that are possible to install the tracking filter inside, there is a concern about a double tracking problem such as temporal correlation of measurements [36]. However, since the proposed tracking algorithm uses different type of process models to the general tracking system, we do not need to seriously concern about the double tracking problem. The proposed algorithm uses vehicle dynamic models constraints on the roadway geometry as the process model, whereas the general tracking filter on the detection sensors uses simple motion model (such as constant velocity and acceleration model) as the process models based on the Cartesian coordinate.

Heterogeneous sensors can have different sampling times which can degrade the entire performance of the fusion-based tracking if we do not consider the synchronization of each sensor. There are two approaches to solve the synchronization problem: software and hardware approaches. The software approach compensates for the mismatched time of the each sensor by using compensation algorithms [37]–[39]. This method does not need an additional hardware system for the synchronization, but the overall algorithm can be complicated. The hardware approach uses a special synchronization system (such as a synchronization clock and pulse module) to synchronize each sensor. Although this approach requires an additional device to synchronize, it is a convenient and reliable method for the synchronization of the tracking system.

In this paper, we used four LIDARs for the moving vehicle detection (Fig. 2). Since each LIDAR provides the same data structure, the consistent measurement vector list can be generated without data format conversion. The measurement vector is composed of the position and velocity information in vehicle body coordinates, as shown in equation (1).

$$z_k = [x \quad y \quad v_x \quad v_y]. \tag{1}$$

The noise feature of the LIDAR was analyzed before the implementation and applied to the measurement covariance matrix design. Since the LIDAR manufacturer provides the synchronization system using the synchronization pulse, it is possible to synchronize each LIDAR without an additional compensation algorithm.

IV. Curvilinear Coordinate Conversion

There are two basic traffic rules for roadway driving. The first one is that the vehicle should follow the predefined roadway while remaining within the lane. The other one is that a vehicle must change lanes within certain road boundaries. Based on these traffic rules, it is possible to set roadway geometry constraints for the motion of moving vehicles on the roadway. The road geometry constraints can help to simplify and reduce the complexities of the problem related to moving vehicle motions on the roadway. In this paper, in order to apply the roadway geometry constraints into the vehicle motion, a *curvilinear coordinate system* is used as a basic coordinate system for the vehicle motion tracking and reasoning algorithms.

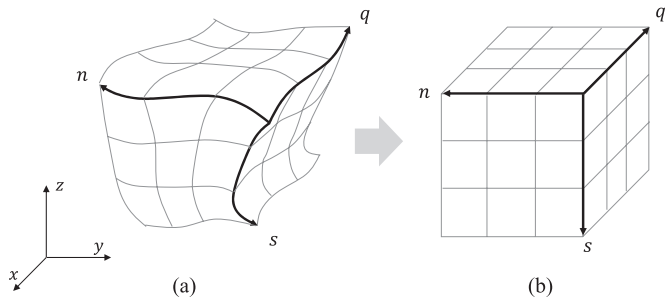

Fig. 3. Curvilinear coordinates can be represented by the orthogonal computing space.

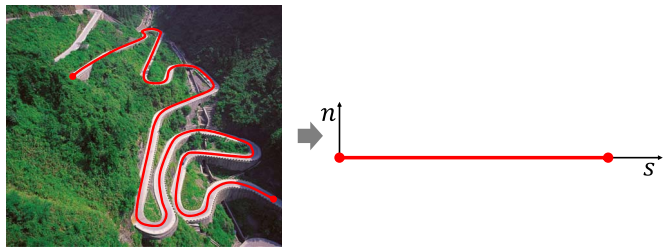

Fig. 4. Roadway-based curvilinear coordinates can simplify the complex vehicle motion problems using the orthogonal computing space.

A. Curvilinear Coordinate System Based on Roadway Geometry

The curvilinear coordinate system is described in Euclidean space in which the one or more coordinate axes are represented based on a curved geometry, as shown in Fig. 3(a). The x, y, and z in Cartesian coordinates can be converted to the orthogonal space of curvilinear coordinate represented by s, n, and q. The curvilinear coordinates can be represented by the orthogonal computing space, as shown in Fig. 3(b). Due to the orthogonality of the computing space, it is possible to make the motion-related problems constrained on the curvilinear coordinates easier.

These curvilinear coordinates can be applied for vehicle motion problems occurring on the roadway. The curvilinear coordinates can be constructed based on the roadway geometry from the roadway map database. Fig. 4 shows an example of the curvilinear coordinate system based on the roadway geometry. Complex vehicle motions in a complex roadway [Fig. 4(a)] can be converted into a simple motion on the two-dimensional orthogonal computing space [Fig. 4(b)]. The conversion into roadway-based curvilinear coordinates reduces the complexity of the vehicle motion problems by changing it into problems on the orthogonal space.

B. Curvilinear Coordinate Conversion of Measurements

Fig. 5 shows a schematic of the conversion process for the vehicle detection measurements from on-board sensors into the roadway-constrained curvilinear coordinate system. Three types of coordinate systems are related to the conversion

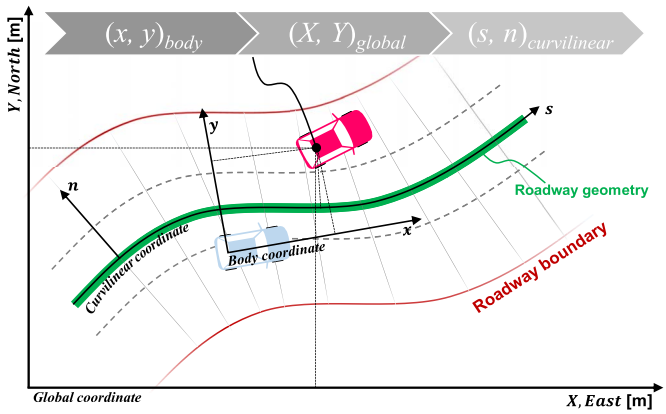

Fig. 5. Roadway geometry-based curvilinear coordinate conversion of vehicle measurements.

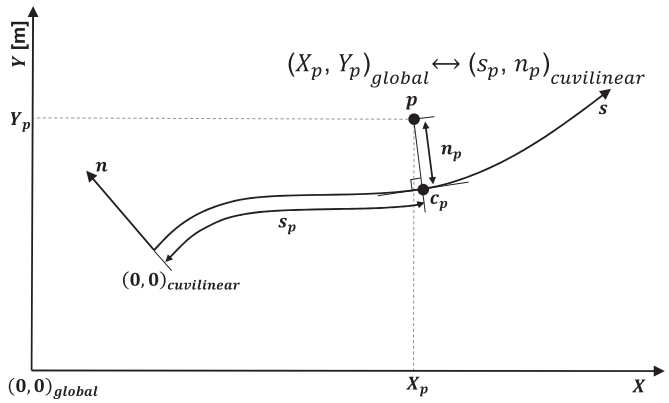

Fig. 6. Coordinate conversion from the global Cartesian coordinate system to the roadway-based curvilinear coordinate system.

process: global Cartesian coordinate, roadway-based curvilinear coordinate, and vehicle body Cartesian coordinate systems.

1) Vehicle Body Cartesian Coordinate System $(x, y)_{\text{body}}$*:* The position and velocity information of the target vehicle (magenta vehicle in Fig. 5) are represented using the vehicle body Cartesian coordinates referenced on the vehicle body frame. The axes of the body Cartesian coordinates are composed of the longitudinal axis (x) and lateral axis (y) in metric units.

2) Global Cartesian Coordinate System $(X, Y)_{\text{global}}$*:* The axes of the global Cartesian coordinate system consist of east and north in metric units, as shown in Fig. 5. The roadway geometry curve and ego vehicle position are represented on the global Cartesian coordinate system. The roadway geometry curve is described using the B-spline curve model from the roadway map database. The control points for the roadway B-spline curve are represented in the global Cartesian coordinates. The localization system of the ego vehicle also provides its position and heading states in the global Cartesian coordinates.

3) Roadway-Based Curvilinear Coordinate System $(s, n)_{\text{curvilinear}}$*:* The roadway-based curvilinear coordinate system can be constructed based on the roadway geometry curve from the map database. The axes of the curvilinear coordinate system are composed of the longitudinal (s) and lateral (n) axes along the roadway geometry, as shown in Fig. 5.

As shown in Fig. 6, a point $(X_p, Y_p)_{\text{global}}$ on the global Cartesian coordinate system can be converted into a point $(s_p, n_p)_{\text{curvilinear}}$ on the curvilinear coordinate system by finding the closest point, c_p, on the roadway geometry curve model. The arc length from the origin of the roadway curve $(0, 0)_{\text{curvilinear}}$ to the closest point, c_p, is converted to s_p and the distance to the closest point is represented as n_p. The closest point is calculated by using a numerical technique that combines quadratic minimization and Newton's method [40], which minimizes the distance between the point and the curve. The vector from c_p to $(X_p, Y_p)_{\text{global}}$ is perpendicular to the tangential vector of the roadway geometry curve at c_p. By using this orthogonality, an inverse coordinate conversion from the point $(s_p, n_p)_{\text{cuvilinear}}$ to the point $(X_p, Y_p)_{\text{global}}$ can be simply performed.

4) Curvilinear Coordinate Conversion: In order to represent the vehicle measurements in the curvilinear coordinate system, the vehicle measurements $(x, y)_{\text{body}}$ represented in the body Cartesian coordinate system should be converted into the global Cartesian coordinate system $(X, Y)_{\text{global}}$ first. The conversion from the body to global Cartesian coordinates is performed based on the ego vehicle position and heading information from the localization system. After the global Cartesian coordinate conversion, it is possible to convert the vehicle measurement into curvilinear coordinates $(s, n)_{\text{curvilinear}}$ by using the closest point finding method. The results of the curvilinear coordinate conversion for the vehicle measurement can be used for filtering the vehicle measurements which are located on the outside of the roadway boundary of interest.

V. Unified Vehicle Tracking and Behavior Reasoning Based on an Interacting Multiple Model (IMM) Filter

A. Limitations of Conventional Vehicle Tracking and Behavior Reasoning Algorithms

Most conventional vehicle tracking systems use Cartesian-coordinate based dynamic models for the prediction of vehicle motion. The state of the dynamic models normally consists of position (x, y), velocity (v_x, v_y), acceleration (a_x, a_y), heading (ψ), and turn rate (γ). The limitation of the Cartesian-coordinate based dynamic model is that it considers all the possible directions of the vehicle motion even though the most plausible vehicle motion can be inferred from the predefined roadway geometry, as shown in Fig. 7. The unnecessary consideration of the high-order degree-of-freedom motion of vehicles can degrade the performance of the tracking algorithm by increasing the uncertainty of the prediction. Therefore, in order to improve the accuracy and reliability of the tracking algorithm, the vehicle motion model constrained on the roadway geometry should be applied to the vehicle tracking algorithms.

There is another limitation when the Cartesian coordinate-based tracking algorithm is applied to behavior reasoning problems without roadway geometry constraints. If the behavior reasoning algorithm does not have the roadway geometry information, it is very hard to classify the vehicle behavior only based on the motion information of vehicles. For instance, the two vehicles in Fig. 8 have the same vehicle motion but come from different intentions: one which follows the curved

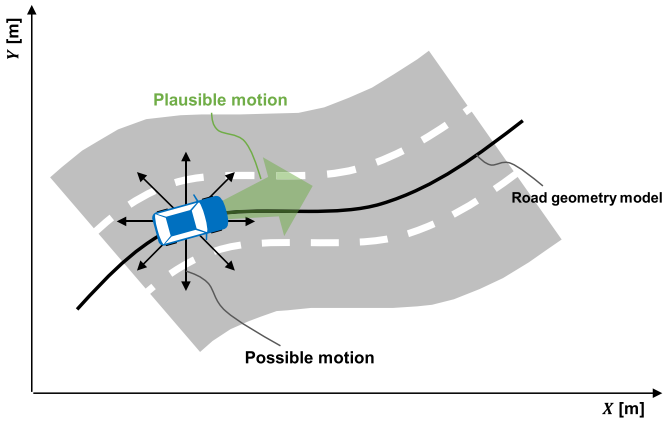

Fig. 7. Vehicle motions on the roadway including possible and plausible motions.

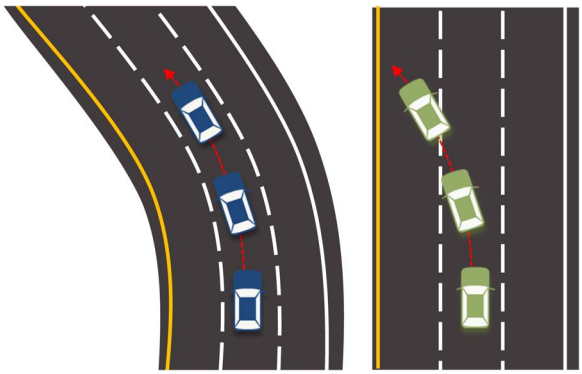

Fig. 8. Same vehicle motion can be interpreted differently.

path and one which changes lanes. To classify the vehicle intention and behavior more accurately, the roadway geometry constraints should be considered in the reasoning algorithm.

B. Motion Tracking and Behavior Reasoning Problems in the Curvilinear Coordinate System

In order to set up the roadway geometry constraints for the vehicle tracking and behavior reasoning algorithm, the curvilinear coordinate system is applied to the algorithm. The curvilinear coordinate system consists of the longitudinal axis (s) and lateral axis (n). The vehicle motion on the curvilinear coordinate system can be represented as longitudinal and lateral states: position (s, n), velocity (v_s, v_n), and acceleration (a_s, a_n) (Fig. 9).

The conversion of tracking problems in the curvilinear coordinate system is very effective to design the uncertainty features of the prediction model (covariance matrix of the prediction model) of the tracking filter. The vehicle motion along the longitudinal direction (s-axis) normally has a wide dynamic range due to acceleration and braking. Therefore, the covariance parameters of the longitudinal states (s, v_s, a_s), which represent the uncertainty feature of the states, should be designed to represent a wide dynamic range maneuver ($<$10 m/s^2) [41], [42]. On the contrary to the longitudinal vehicle motion, the lateral vehicle motion on the n-axis usually has a narrow dynamic range in the roadway driving conditions because the

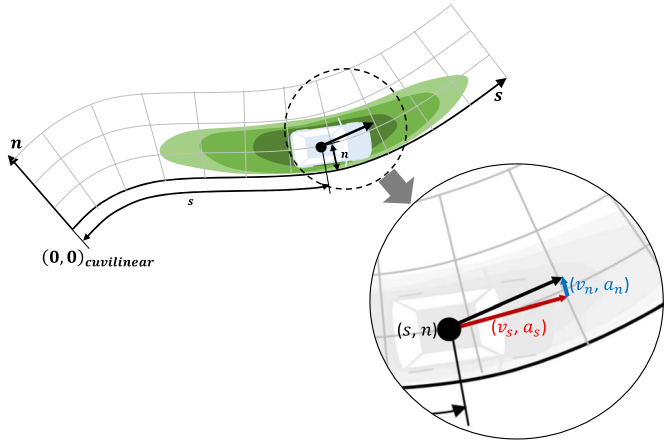

Fig. 9. The vehicle motion in the curvilinear coordinate system can be represented using the position (s, n), velocity (v_s, v_n), and acceleration (a_s, a_n). The probabilistic distribution of the vehicle motion is represented as the greenish region.

lateral motion occurs in lane changing situations and the dynamic feature of the lane changing is not large ($<$ 2 m/s^2) [41], [42]. Therefore, the covariance parameters of the lateral states (n, v_n, a_n) of the tracking filter can be designed to be small ($<$ 2 m/s^2) to cover the narrow dynamic range maneuver. By applying the covariance design method to the tracking filter, we can obtain the probabilistic distribution of vehicle motions, as shown in Fig. 9.

In addition to the simplicity of the uncertainty parameter design for the tracking filter, the curvilinear coordinate system can provide a good feature to classify the lateral behavior of vehicles such as lane keeping and lane changing. The lateral speed, v_n, and acceleration, a_n, in curvilinear coordinates are directly related to lane changing motion. Therefore, it is easy to classify the lane changing behavior from lane keeping behaviors by using the lateral speed, v_n, and acceleration, a_n, in the curvilinear coordinate system. The curvilinear coordinate-based behavior classification can also work well in curved roadway environments, as shown in Fig. 8, even though the vehicle motions are the same in the Cartesian coordinate system.

However, there should be caution when using the curvilinear coordinate system for vehicle tracking and behavior reasoning problems. Since the curvilinear coordinate system is constructed based on roadway geometry from the map and the curvilinear coordinate conversion is performed using the global positions of the ego vehicle, the uncertainty of the roadway map and localization should be considered in the filter design. The accuracy and noise characteristics of the localization and roadway geometry map should be analyzed before the tracking filter design and the results should be added to the measurement covariance of the tracking filter. The recommend accuracy of the localization and roadway geometry for the curvilinear coordinate system is lane-level accuracy (about $<$ 0.3 meter).

C. IMM Filter-Based Unified Motion Tracking and Behavior Reasoning

The purpose of interacting multiple-model (IMM) filters is to cope with maneuvering targets [43]. The maneuvering means that the motion of the target is not matched by the predicted

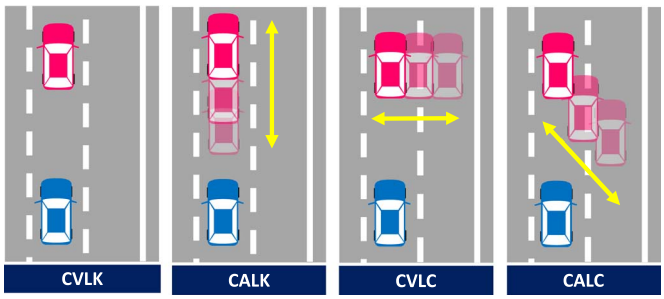

Fig. 10. Curvilinear coordinates can be translated into the orthogonal computational space.

motion of the tracking model due to changing of the target motion behavior. In order to cope with target maneuvering, the IMM filter considers several hypothesis of the prediction model and executes several Kalman filtering algorithms based on the hypothesis (prediction models). The IMM filter can then select the appropriate prediction model for the current target motion by applying a probabilistic approach to the each filtering result and estimate the target state based on the selected appropriate model. Since the tracking states are estimated based on the appropriate hypothesis, the accuracy and reliability of the estimation can be improved.

This filtering procedure of the IMM filter which selects the appropriate behavior model and applies it to the tracking can be applied to the *unified* vehicle tracking and behavior reasoning algorithm. For the behavior reasoning, the vehicle behaviors that we want to classify, such as lane keeping and lane changing, are defined and modeled with mathematical representations. By implementing the IMM filter based on the designed behavior model, we can classify the behavior of the target vehicle by using the probabilistic classification process of the IMM filter. At the same time, the vehicle tracking performance can be improved by adapting the proper vehicle motion model to the tracking filter.

1) Vehicle Motion Model-Set: The proposed tracking and behavior reasoning algorithm is designed for the *normal on-road driving* situations where the roadway geometry map is available. In order to cover the driving behaviors for the normal driving on the on-road, we classify the vehicle motion model into four groups by considering the longitudinal and lateral motion features in the curvilinear coordinate system, as shown in Fig. 10. The vehicle model set is composed of CVLK, CALK, constant velocity lane changing (CVLC), and constant acceleration lane changing (CALC) models.

a) Constant velocity lane keeping (CVLK) model: The CVLK motion represents the most stable driving condition on the roadway. Since there is no acceleration or braking, the longitudinal motion can be represented by only using the longitudinal position (s) and speed (v_s). In addition, the lateral speed, v_n, and acceleration, a_n, of a vehicle in the curvilinear coordinates can be ignored because the vehicle remains in the lane. The CVLK motion can be described as shown in equation (2).

$$\begin{bmatrix} s \\ n \\ v_s \end{bmatrix}_k = \begin{bmatrix} 1 & 0 & \Delta t \\ 0 & 1 & 0 \\ 0 & 0 & 1 \end{bmatrix} \begin{bmatrix} s \\ n \\ v_s \end{bmatrix}_{k-1} + \begin{bmatrix} \Delta t^2/2 \cdot w_{a_s} \\ \Delta t^2/2 \cdot w_{a_n} \\ \Delta t \cdot w_{a_s} \end{bmatrix}$$
$$\text{where } w_{a_s} \sim N\left(0, \sigma_{a_s}^2\right) \text{ and } w_{a_n} \sim N\left(0, \sigma_{a_n}^2\right). \quad (2)$$

b) Constant acceleration lane keeping (CALK) model: The CALK motion represents the acceleration and braking motion with lane keeping. Therefore, the longitudinal acceleration, a_s, is additionally required to represent the acceleration and braking. Since the vehicle remains in the lane as in the CVLK model, the lateral speed, v_n, and acceleration, a_n, are not necessary for the CALK model. The CALK motion can be described by equation (3).

$$\begin{bmatrix} s \\ n \\ v_s \\ a_s \end{bmatrix}_k = \begin{bmatrix} 1 & 0 & \Delta t & \Delta t^2/2 \\ 0 & 1 & 0 & 0 \\ 0 & 0 & 1 & \Delta t \\ 0 & 0 & 0 & 1 \end{bmatrix} \begin{bmatrix} s \\ n \\ v_s \\ a_s \end{bmatrix}_{k-1} + \begin{bmatrix} \Delta t^2/2 \cdot w_{a_s} \\ \Delta t^2/2 \cdot w_{a_n} \\ \Delta t \cdot w_{a_s} \\ w_{a_s} \end{bmatrix}$$
$$\text{where } w_{a_s} \sim N\left(0, \sigma_{a_s}^2\right) \text{ and } w_{a_n} \sim N\left(0, \sigma_{a_n}^2\right). \quad (3)$$

c) Constant velocity lane changing (CVLC) model: The CVLC model represents lane changing motion with a constant velocity. In order to represent the lateral motion of lane changing, the lateral vehicle speed, v_n, is required for the CVLC model. Since there is no acceleration or braking for the motion, the longitudinal motion can be represented by only using the longitudinal position (s) and speed (v_s). The CVLC motion can be described by equation (4).

$$\begin{bmatrix} s \\ n \\ v_s \\ v_n \end{bmatrix}_k = \begin{bmatrix} 1 & 0 & \Delta t & 0 \\ 0 & 1 & 0 & \Delta t \\ 0 & 0 & 1 & 0 \\ 0 & 0 & 0 & 1 \end{bmatrix} \begin{bmatrix} s \\ n \\ v_s \\ v_n \end{bmatrix}_{k-1} + \begin{bmatrix} \Delta t^2/2 \cdot w_{a_s} \\ \Delta t^2/2 \cdot w_{a_n} \\ \Delta t \cdot w_{a_s} \\ \Delta t \cdot w_{a_n} \end{bmatrix}$$
$$\text{where } w_{a_s} \sim N\left(0, \sigma_{a_s}^2\right) \text{ and } w_{a_n} \sim N\left(0, \sigma_{a_n}^2\right). \quad (4)$$

d) Constant acceleration lane changing (CALC) model: The CALC motion model represents the most aggressive driving motion. The CALC consider all possible motions (s, n, v_s, v_n, a_s, and a_n) in the curvilinear coordinate system. The CALC motion is described by equation (5).

$$\begin{bmatrix} s \\ n \\ v_s \\ v_n \\ a_s \\ a_n \end{bmatrix}_k = \begin{bmatrix} 1 & 0 & \Delta t & 0 & \frac{\Delta t^2}{2} & 0 \\ 0 & 1 & 0 & \Delta t & 0 & \frac{\Delta t^2}{2} \\ 0 & 0 & 1 & 0 & \Delta t & 0 \\ 0 & 0 & 0 & 1 & 0 & \Delta t \\ 0 & 0 & 0 & 0 & 1 & 0 \\ 0 & 0 & 0 & 0 & 0 & 1 \end{bmatrix} \begin{bmatrix} s \\ n \\ v_s \\ v_n \\ a_s \\ a_n \end{bmatrix}_{k-1} + \begin{bmatrix} \Delta t^2/2 \cdot w_{a_s} \\ \Delta t^2/2 \cdot w_{a_n} \\ \Delta t \cdot w_{a_s} \\ \Delta t \cdot w_{a_n} \\ w_{a_s} \\ w_{a_n} \end{bmatrix}$$
$$\text{where } w_{a_s} \sim N\left(0, \sigma_{a_s}^2\right) \text{ and } w_{a_n} \sim N\left(0, \sigma_{a_n}^2\right). \quad (5)$$

Here, w_a represents the noise due to the unexpected acceleration, which can be modeled as a Gaussian normal distribution with a zero mean and variance (σ_a) of acceleration. The variance, σ_a^2, can be designed by considering the dynamic characteristics of the vehicle motion on the roadway. The standard deviation of longitudinal acceleration, σ_{a_s}, can be designed

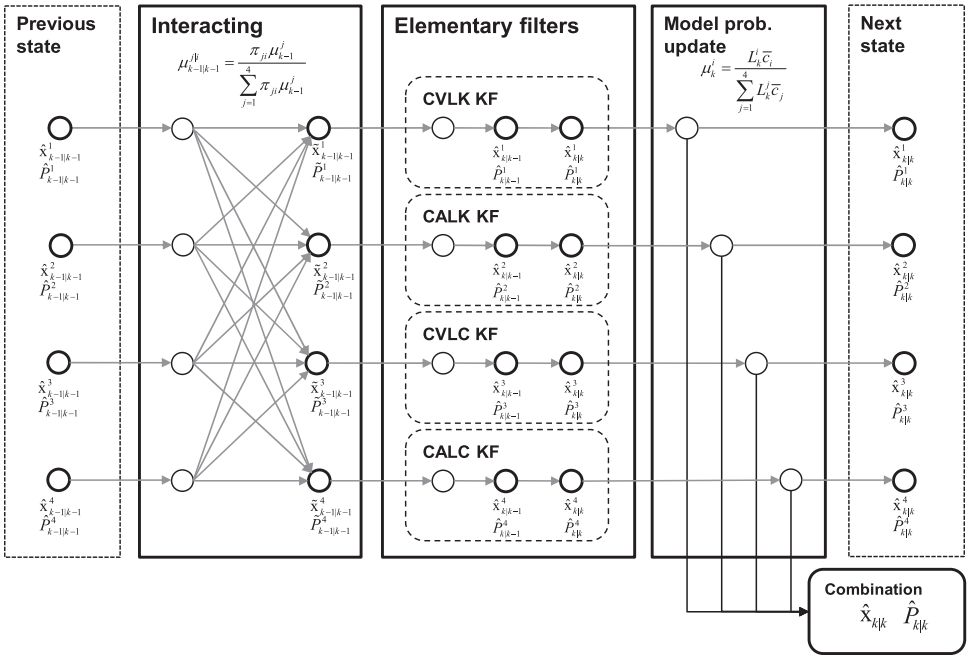

Fig. 11. Overall process of the IMM filter-based vehicle tracking and behavior reasoning.

to be large ($\approx$ 10 m/s^2) to represent the wide dynamic range motion for the longitudinal direction. The standard deviation of the lateral acceleration, σ_{a_n}, can be designed to be small ($\approx$ 2 m/s^2) to represent the narrow dynamic range of the lateral motion. Based on the noise variance of the longitudinal and lateral accelerations, the prediction covariance matrix of each model can be designed as shown in equations (6)–(9). Although the CVLK motion is the most constrained motion model, it has the smallest noise characteristics for model prediction. The CALC has the highest degree of freedom for the motion, but it has the largest uncertainty characteristics among the motion models, given in (6)–(9), shown at the bottom of the page.

2) IMM Filtering for Unified Motion Tracking and Reasoning: Based on the vehicle motion models, we can simultaneously perform the tracking and behavior reasoning by applying the models to the IMM filter. Fig. 11 shows the overall process of the IMM filter-based unified vehicle motion tracking and behavior reasoning. The IMM filter process consists of four steps: interacting, elementary filters, model probability update, and combination.

In the *interacting* step, the state of the previous step of each model is mixed based on the model probability, μ, and model transition probability, π. The model probability, μ, represents the suitability of the each model for the current situation and

$$Q_{\mathrm{CVLK}} = \begin{bmatrix} \Delta t^4/4 \cdot \sigma_{a_s}^2 & 0 & \Delta t^3/2 \cdot \sigma_{a_s}^2 \\ 0 & \Delta t^4/4 \cdot \sigma_{a_n}^2 & 0 \\ \Delta t^3/2 \cdot \sigma_{a_s}^2 & 0 & \Delta t^2 \cdot \sigma_{a_s}^2 \end{bmatrix} \tag{6}$$

$$Q_{\mathrm{CALK}} = \begin{bmatrix} \Delta t^4/4 \cdot \sigma_{a_s}^2 & 0 & \Delta t^3/2 \cdot \sigma_{a_s}^2 & \Delta t^2/2 \cdot \sigma_{a_s}^2 \\ 0 & \Delta t^4/4 \cdot \sigma_{a_n}^2 & 0 & 0 \\ \Delta t^3/2 \cdot \sigma_{a_s}^2 & 0 & \Delta t^2 \cdot \sigma_{a_s}^2 & \Delta t \cdot \sigma_{a_s}^2 \\ \Delta t^2/2 \cdot \sigma_{a_s}^2 & 0 & \Delta t \cdot \sigma_{a_s}^2 & \sigma_{a_s}^2 \end{bmatrix} \tag{7}$$

$$Q_{\mathrm{CVLC}} = \begin{bmatrix} \Delta t^4/4 \cdot \sigma_{a_s}^2 & 0 & \Delta t^3/2 \cdot \sigma_{a_s}^2 & 0 \\ 0 & \Delta t^4/4 \cdot \sigma_{a_n}^2 & 0 & \Delta t^3/2 \cdot \sigma_{a_n}^2 \\ \Delta t^3/2 \cdot \sigma_{a_s}^2 & 0 & \Delta t^2 \cdot \sigma_{a_s}^2 & 0 \\ 0 & \Delta t^3/2 \cdot \sigma_{a_n}^2 & 0 & \Delta t^2 \cdot \sigma_{a_n}^2 \end{bmatrix} \tag{8}$$

$$Q_{\mathrm{CALC}} = \begin{bmatrix} \frac{\Delta t^4}{4} \cdot \sigma_{a_s}^2 & 0 & \frac{\Delta t^3}{2} \cdot \sigma_{a_s}^2 & 0 & \frac{\Delta t^2}{2} \cdot \sigma_{a_s}^2 & 0 \\ 0 & \frac{\Delta t^4}{4} \cdot \sigma_{a_n}^2 & 0 & \frac{\Delta t^3}{2} \cdot \sigma_{a_n}^2 & 0 & \frac{\Delta t^2}{2} \cdot \sigma_{a_n}^2 \\ \frac{\Delta t^3}{2} \cdot \sigma_{a_s}^2 & 0 & \Delta t^2 \cdot \sigma_{a_s}^2 & 0 & \Delta t \cdot \sigma_{a_s}^2 & 0 \\ 0 & \frac{\Delta t^3}{2} \cdot \sigma_{a_n}^2 & 0 & \Delta t^2 \cdot \sigma_{a_n}^2 & 0 & \Delta t \cdot \sigma_{a_n}^2 \\ \frac{\Delta t^2}{2} \cdot \sigma_{a_s}^2 & 0 & \Delta t \cdot \sigma_{a_s}^2 & 0 & \sigma_{a_s}^2 & 0 \\ 0 & \frac{\Delta t^2}{2} \cdot \sigma_{a_n}^2 & 0 & \Delta t \cdot \sigma_{a_n}^2 & 0 & \sigma_{a_n}^2 \end{bmatrix} \tag{9}$$

the model transition probability, π, describes the probability that one model will make a transition to another model. At the *elementary filter*s step, individual Kalman filtering is performed based on each motion model. By using the likelihood, L, from each filtering, the model probability, μ, can be updated in the *model probability update* step. At the *combination* step, the integrated state and covariance are calculated based on a Gaussian mixture equation. The details of the equation of the IMM filter are described in the Appendix.

The model probability, μ, which describes the suitability of the motion model for the current driving conditions, is used to determine the behavior of the target vehicle. The motion model which has the largest model probability, μ, is selected as the current behavior of the target vehicle. The tracking performance for the surrounding vehicles can be improved by using the IMM filter because the filtering result based on the model with the high model probability is weighted more than the other filtering results at the combination step.

VI. Experiments

The experiments were performed on the steering performance test track of the Korea Automobile Testing and Research Institute (KATRI) located in Hwaseong-si, Gyeonggi-do, Korea [Fig. 12(a)]. The steering performance test track [Fig. 12(b)] contains *all types of curvature variance* in the real road situation in order to verify the steering dynamics of vehicle. Due to this curvature variety, the test track also is the best to evaluate the proposed algorithm for the various roadway geometry constraints. In addition, the test road has weed plants on the roadside, which can act as noise of the LIDAR. Therefore, this site is suitable to evaluate the reliability of the tracking algorithm regarding the noise of the LIDAR.

The performance of the vehicle tracking can be evaluated by comparing the tracking estimates with the reference (true) state. However, since it is not possible to know the true state, we developed a *tracking evaluation system* which can provide very accurate reference state of tracking by applying the high-performance positioning systems which integrate a real-time kinematics (RTK) GPS and an inertial measurement unit (IMU). The process of the tracking evaluation system consists of three steps. The *first step* is the measuring of the position and heading direction for the ego and target vehicle. Two high-performance positioning systems (RTK GPS/IMU fusion system) were installed on the ego and target vehicle, respectively, as shown in Fig. 13. From the positioning systems, we can obtain the very accurate position (centimeter level) and heading direction (< 0.1 degrees) for the ego and target vehicle on the global coordinate. The *second step* is the synchronization of the two measurements from the ego and target vehicle. Since the positioning system provides the global GPS time, it is possible to synchronize the position and heading direction measurement of the ego and target vehicle. The *final step* is the calculation of the reference tracking state from the synchronized ego and target measurements. The reference tracking state is the local position and heading direction of target vehicle on the local coordinates of the ego vehicle, as shown in Fig. 13. From the synchronized measurements for the ego and target vehicle, we can obtain the reference tracking state by coordinate converting the target vehicle measurement to the ego vehicle local coordinate centered on the ego vehicle measurement.

(a)

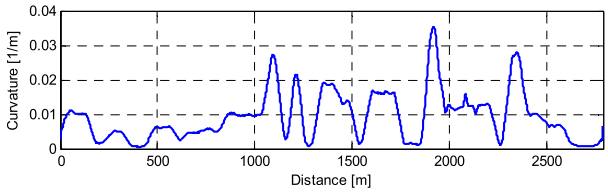

(b)

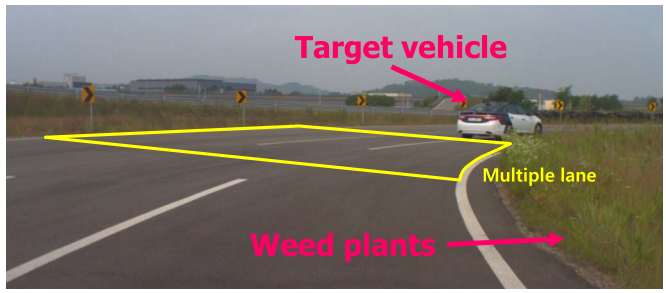

(c)

Fig. 12. The test road has various curvatures with multiple lanes in order to verify the unified vehicle tracking and behavior reasoning algorithm. There are weed plants on the roadside of the test road. These conditions are appropriate to evaluate the accuracy and reliability of the proposed algorithm.

A. Evaluation of the Tracking and Behavior Reasoning

To evaluate the proposed tracking and behavior reasoning algorithm in the various situations, the experiments were classified into four scenarios: constant velocity lane keeping (CVLK), constant acceleration lane keeping (CALK), constant velocity lane changing (CVLC), and constant acceleration lane changing (CALC) scenarios.

1) Constant Velocity Lane Keeping (CVLK) Scenario: The target vehicle state for the constant velocity and lane keeping (CVLK) scenario is shown in Fig. 14. The vehicle speed is about 40 km/h and the longitudinal acceleration is almost zero to emulate the constant velocity scenario. The steering and yaw rate only exist to trace the curved roadway.

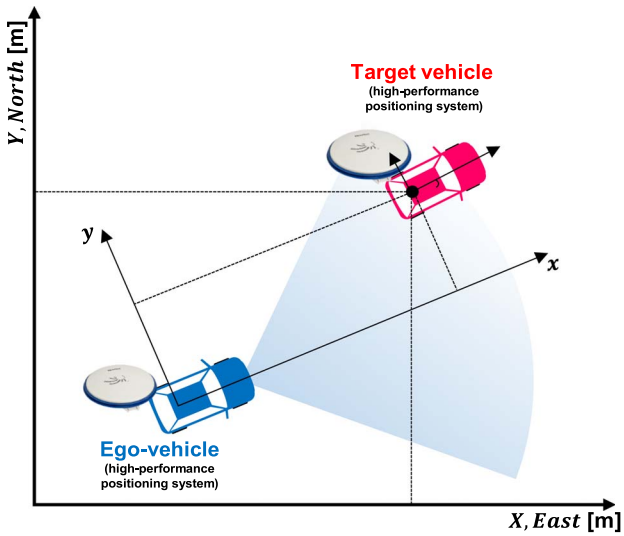

Fig. 13. Tracking algorithm evaluation based on the high-accuracy positioning systems. The reference tracking state (relative distance and heading direction of the target vehicle from the ego-vehicle) can be obtained from the high accuracy positioning systems equipped on the target and ego vehicles.

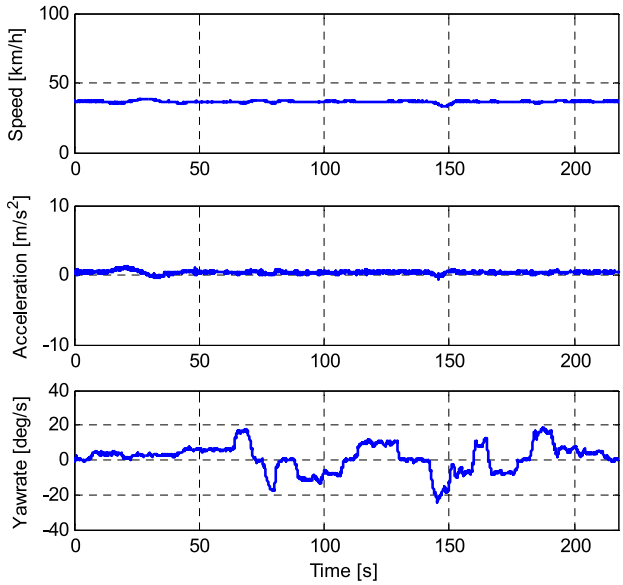

Fig. 14. Vehicle motion state of the target vehicle for the CVLK scenario.

The behavior reasoning result for the CVLK scenario is shown in Fig. 15. Since the speed variance is very small and the target vehicle follows the roadway, the CVLK model probability is dominant compared to the other motion models. Therefore, the behavior reasoning criteria can classify the scenario as CVLK.

The tracking performance can be evaluated by comparing the estimation error with the measurement error. Fig. 16 describes the heading, position and speed errors from the proposed tracking algorithm and measurement, respectively. The measurements are generated from the LIDAR modules which provide the tracking results on the conventional Cartesian coordinate. High accuracy positioning system was used as the reference (Fig. 13). Since the roadway geometry constraints are applied to the measurement, the heading angle estimate of the proposed

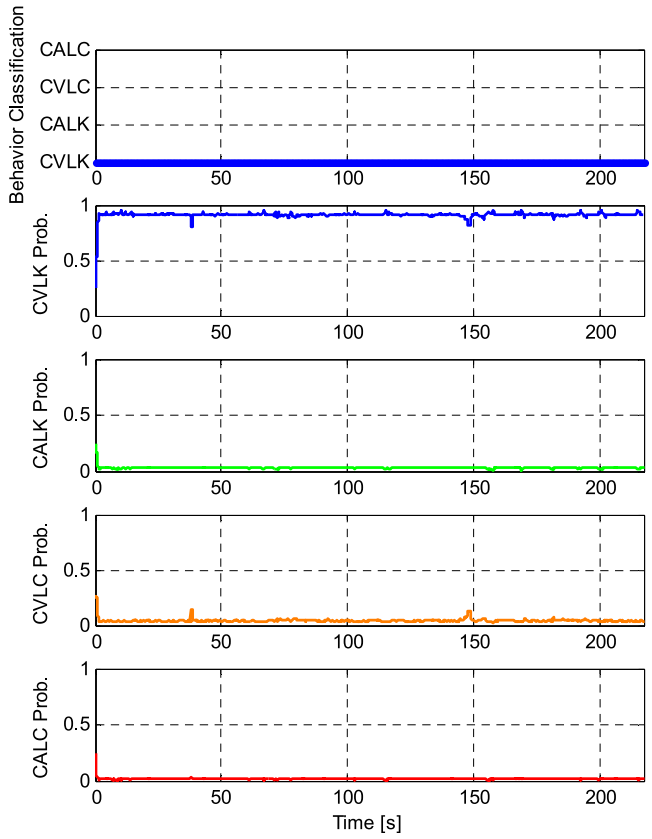

Fig. 15. Behavior reasoning result for the CVLK scenario.

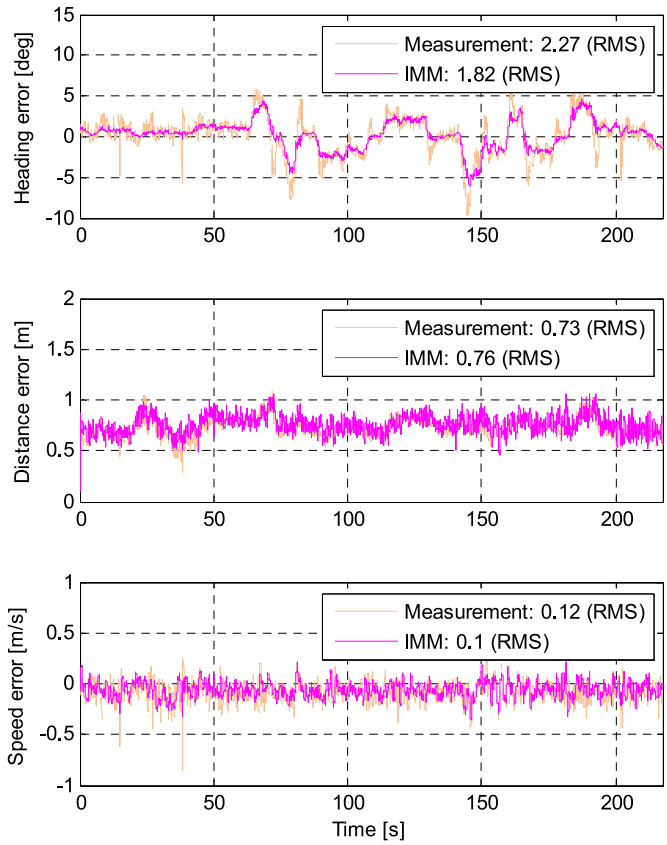

Fig. 16. Estimation errors of the position, heading, and speed state for the CVLK scenario.

tracking and behavior reasoning algorithm (IMM filter) reduced about 20%. This improved performance of the heading angle estimate is beneficial to predict the target vehicle trajectory for the dynamic motion planning algorithm based on a physics-based prediction approach [44].

The accuracy of the position and speed estimation is not improved much compared to the result of heading estimate. This is because the tracking models used for the proposed tracking filter do not consider the noise due to the bounding box association error from the LIDARs. The LIDAR estimates the state of position of target vehicles based on the two steps: the first step is the bounding box association based on the measured laser point clouds reflecting from the surface of the target vehicle, and the second step is the tracking based on the center point of the bounding box association. The problem is that the center position of the bounding box can be changed by the shape pattern variation of the laser point clouds, and the shape pattern can be varied according to the change of the viewpoint of the LIDAR to the target vehicle. Since the viewpoint change does not follow the Gaussian random noise properties, the noise characteristic of the position error due to the change of bounding box center also does not follow the Gaussian noise characteristics. Since the tracking filter used in the proposed IMM filter based on the linear Kalman filter, it is not available to cover the non-Gaussian noise even though we apply the roadway geometry constraints. This problem can only be solved by applying the detection sensors which are invariant to the viewpoint change.

2) Constant Acceleration Lane Keeping (CALK) Scenario: The target vehicle state for the constant acceleration and lane keeping (CALK) scenario is described in Fig. 17. The vehicle speed was oscillated from about 10 km/h to 60 km/h in order to emulate the constant acceleration scenario. Even though the longitudinal acceleration of the target vehicle was not constant, we defined the scenario as constant acceleration because only the constant acceleration motion model can cover the situation. For the lane keeping scenario, the limited variation of the steering input and yaw rate existed to trace the curved roadway.

The behavior reasoning result for the CALK scenario is described in Fig. 18. When the longitudinal acceleration of the target vehicle is large, the CALK model probabilities are dominant compared to the other motion models. The behavior reasoning algorithm based on the IMM filter classifies the behavior as CALK at the situation of the large longitudinal accelerations. However, there are some regions that the reasoning algorithm classifies the behavior as CVLK model in Fig. 18. The ambiguity of the behavior reasoning comes from the experiments constraints. For the experiment of CALK scenario, the test vehicle should maintain the acceleration or braking for the experiment region. However, it is impossible to maintain the acceleration for a long time due to the actuation (engine) limitation, and it is impossible to maintain the braking because the test vehicle will stop. Therefore, the transition between acceleration and braking should exist in order to complete the experiments of the CALK scenario. At the transition region, the acceleration of the test vehicle becomes and maintains almost zero for a short time, and the behavior reasoning algorithm classifies this situation (zero acceleration) as the CVLK behavior.

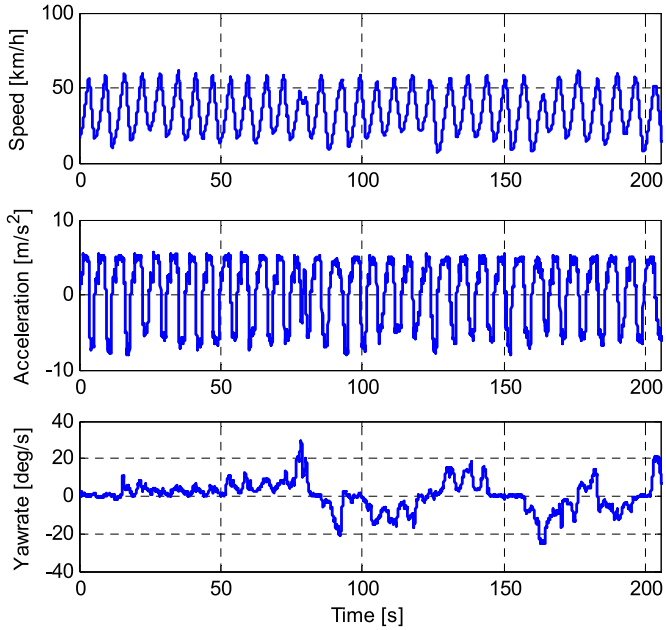

Fig. 17. Vehicle motion state of the target vehicle for the CALK scenario.

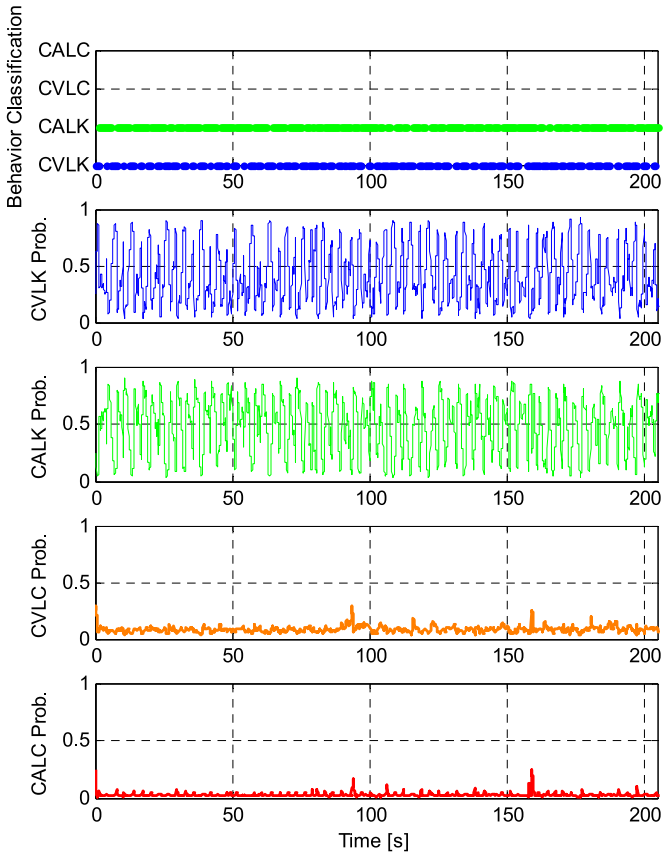

Fig. 18. Behavior reasoning result for the CALK scenario.

The estimation errors of the heading, position and speed are described in Fig. 19. Since the roadway geometry constraints are applied to the target vehicle tracking as in the CVLK scenario, the heading angle estimation error of the IMM filter is reduced about 35% compared to the measurements. This superior tracking performance of the heading angle estimate is also beneficial to predict the target vehicle trajectory for the

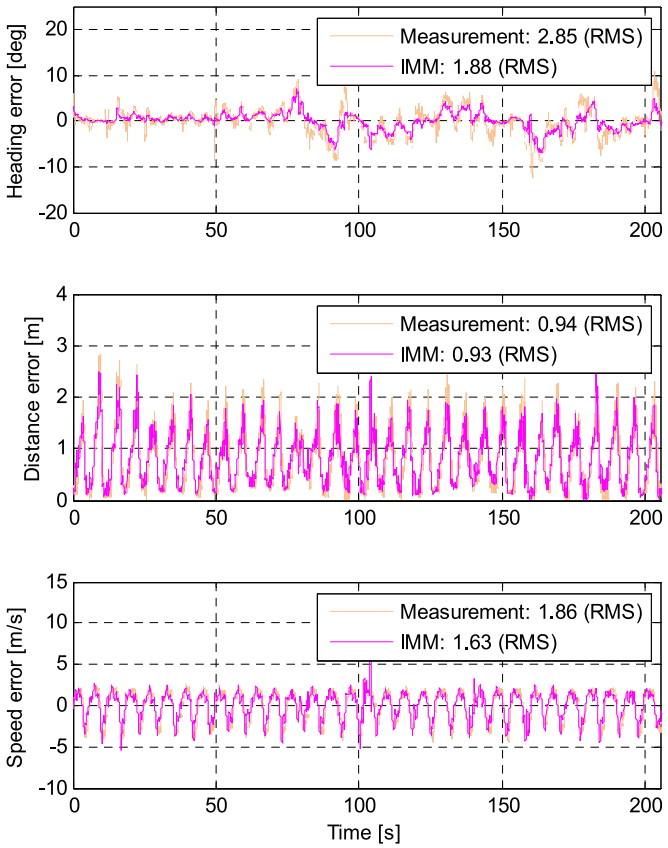

Fig. 19. Estimation errors of the position, heading, and speed state for the CALK scenario.

collision avoidance algorithm. However, the position estimation performance is not improved much to compare to the measurements due to the same reason of the CVLK experiments result.

3) Constant Velocity Lane Changing (CVLC) Scenario: The target vehicle state for the constant velocity and lane changing (CVLC) scenario is described in Fig. 20. The vehicle speed was about 40 km/h and the longitudinal acceleration is almost zero for the constant velocity scenario. The target vehicle continuously changes its lane in order to emulate the lane changing scenario. Therefore, the steering input and yaw rate have frequent changes as shown in the Fig. 20.

The behavior reasoning result for the CVLC scenario is described in Fig. 21. Since the speed variance is very small and the target vehicle changes its lane continuously, the CVLC model probabilities are dominant compared to the other motion models. The behavior reasoning algorithm mostly classifies the scenario as CVLC for the constant velocity and lane changing scenario. There are some miss classifications as CALC, CALK, and CVLK because it is difficult for the test driver to perfectly drive the target vehicles with the constant speed and continuous lane changing simultaneously.

The estimation errors of the heading, position, and speed are described in Fig. 22. Since the roadway geometry constraints are applied to the vehicle tracking, the heading angle estimation error is reduced about 7% compared to the measurements. However, the position estimation performance is not improved to compare to the measurements because of the same reasons described in the CVLK experiments analysis. In addition, since

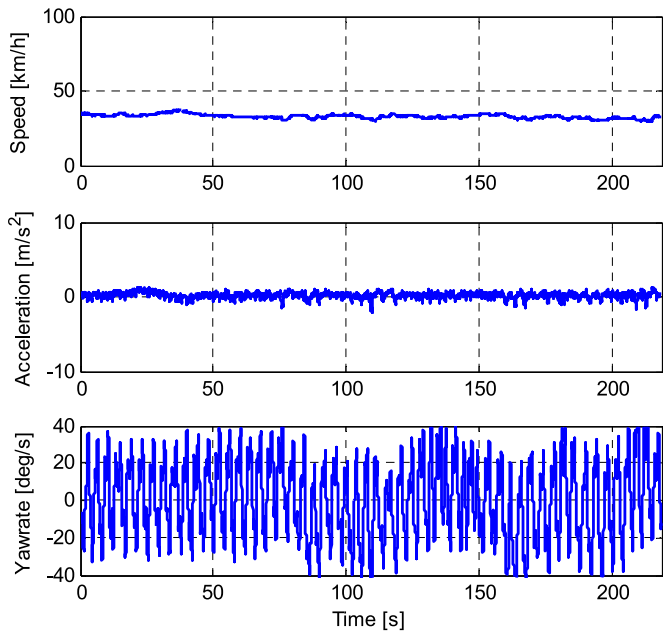

Fig. 20. Vehicle motion state of the target vehicle for the CVLC scenario.

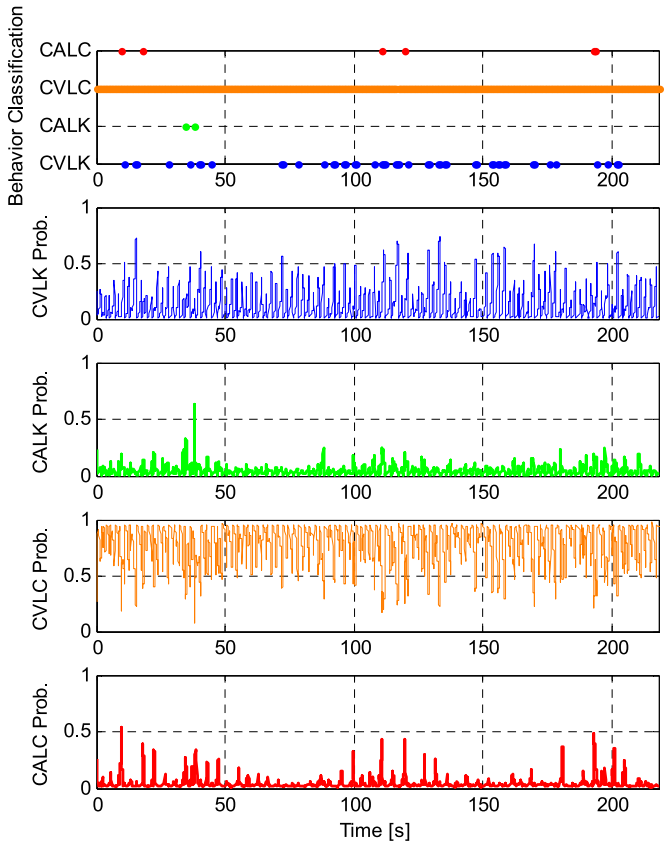

Fig. 21. Behavior reasoning result for the CVLC scenario.

the CVLC model does not consider the lateral acceleration of the vehicle (only considering the lateral velocity), it can amplify the performance degradation when the fast lane changing (high lateral acceleration) is occurred.

4) Constant Acceleration Lane Changing (CALC) Scenario: The target vehicle state for the constant velocity and lane

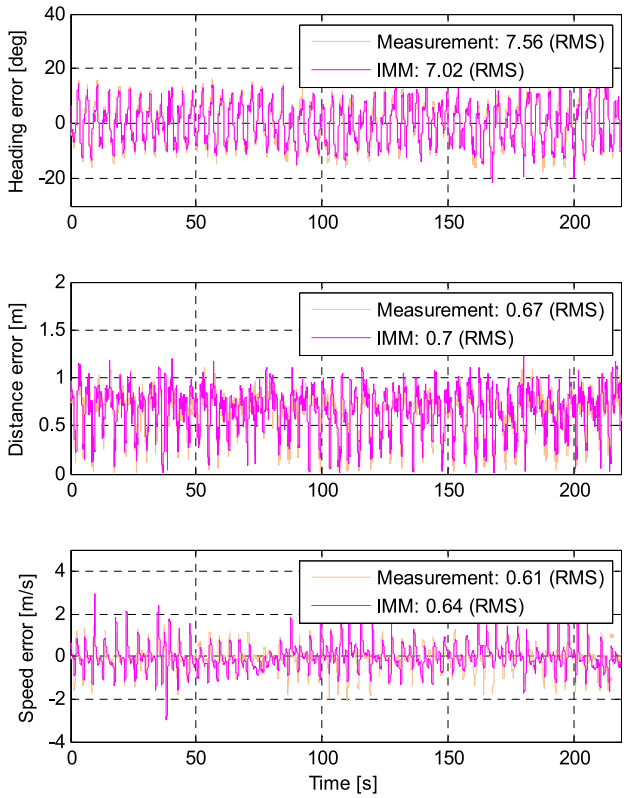

Fig. 22. Estimation errors of the position, heading, and speed state for the CVLC scenario.

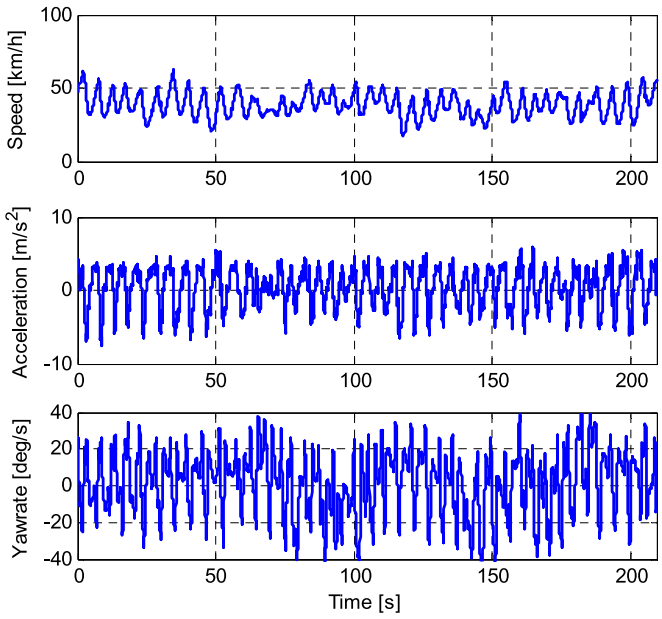

Fig. 23. Vehicle motion state of the target vehicle for CALC scenario.

changing (CALC) scenario is described in Fig. 23. The vehicle speed was oscillated from about 20 km/h to 50 km/h to emulate the constant acceleration, and the target vehicle continuously changes its lane in order to emulate the lane changing scenario.

The behavior reasoning result for the CALC scenario is described in Fig. 24. When the longitudinal acceleration of the target vehicle is large with the lane changing, the CALC model probabilities are increased compared to the other motion

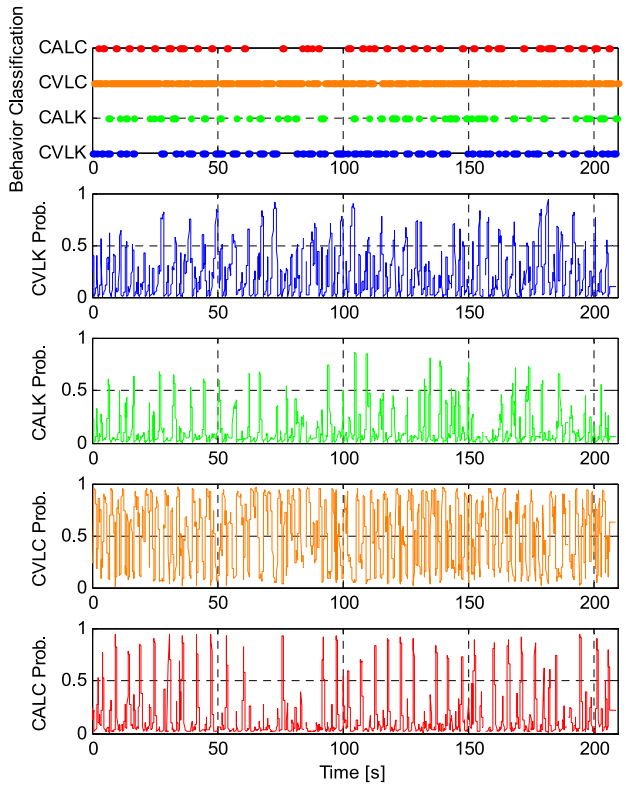

Fig. 24. Behavior reasoning result for the CALC scenario.

models. Therefore, the behavior reasoning algorithm classifies the scenario as CALC at the situation. However, it is ambiguous that the CALC behavior classification is not dominant for the test result of CALC scenario in the Fig. 24. The ambiguity of the behavior reasoning of the CALC scenario comes from the experiments limitation. For the constant acceleration lane changing (CALC) scenario, the test vehicle should maintain the acceleration or braking with lane changing; however, it is very difficult to change the lane with the harsh acceleration or braking simultaneously due to the actuator limitation and test safety issues. Therefore, there are only small numbers of CALC classification for the experiment of CALC scenario. However, the important thing is that the algorithm can classify the aggressive and dangerous driving behavior of the target vehicles which have the CALC behavior. This classification results can be used to plan the safety motion of the autonomous car regarding the aggressive behavior of the surrounding car.

The estimation errors of the heading, position, and speed are described in Fig. 25. Since the roadway geometry constraints are applied to the vehicle tracking, the heading angle estimation error is reduced about 5% compared to the measurements. However, the position estimation performance is not improved to compare to the measurements due to the same reasons described in the previous experiments analysis.

B. Analysis of the Error Effect of the Roadway Geometry on the Tracking and Behavior Reasoning

The proposed algorithm applies the roadway geometry constraints to the tracking and behavior reasoning based on the

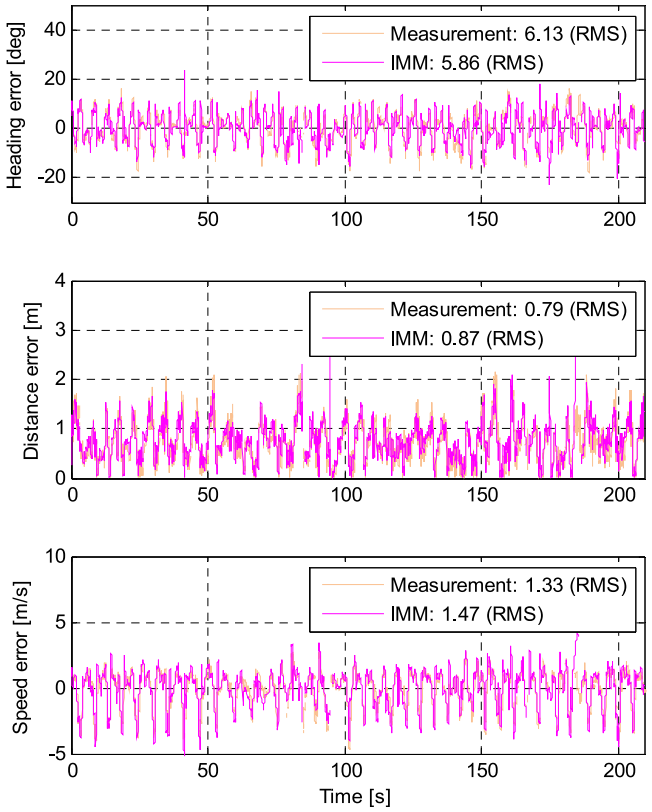

Fig. 25. Estimation error of position and heading state for the CALC scenario.

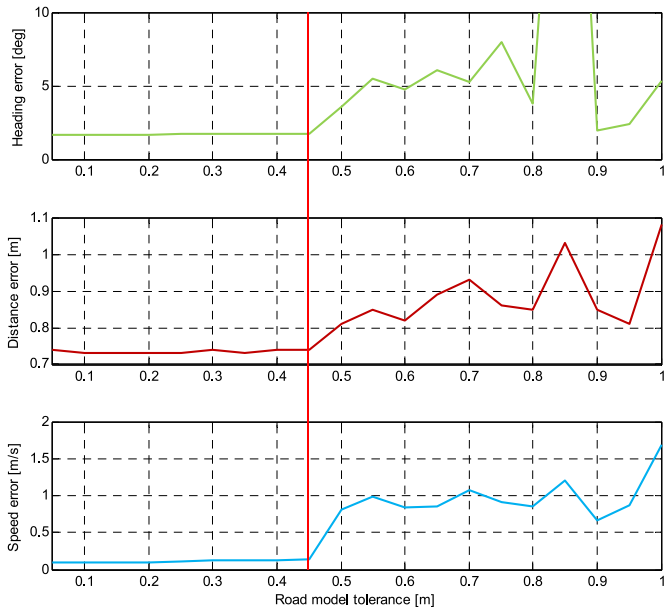

Fig. 26. State estimate errors for the different error boundaries of road geometry map for the tracking algorithm.

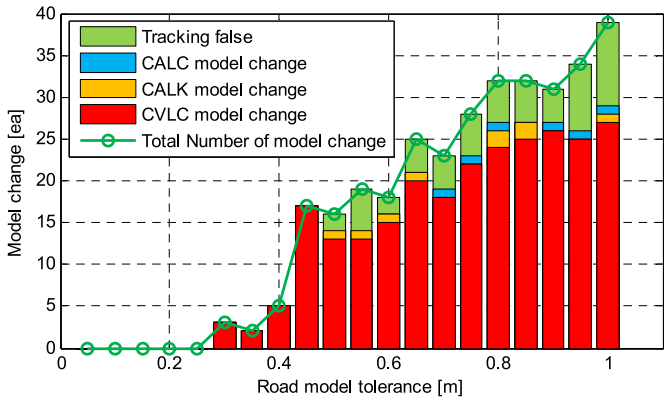

Fig. 27. The number of misclassifications for the incorrect behaviors (such as the CALC, CALK, CVLC, and tracking fail) begins to increase from the 0.25 m of the road model tolerance.

roadway map database. Therefore, the *error of roadway geometry map* can largely affect the performance of the tracking and behavior reasoning. In order to analyze the effect of roadway geometry error, we performed experiments according to the various roadway geometry error.

The map generation algorithm constructs the roadway geometry map database by gradually approximate the post-processed position data from high-accuracy positioning system (centimeter-level) into the B-spline road model *until the error comes within the tolerance range* [35]. Therefore, we can set up the various error boundary of the roadway geometry map by selecting difference tolerance of the map generation algorithm. In this analysis, the error boundaries of the roadway geometry map are from the 0.05 meters to the 1.00 meters with the 0.05 meter interval. We performed the error effect analysis using the experiment data of CVLK scenario because the CVLK model has the greatest impact on the roadway geometry constraint among the four types of scenario.

In order to analyze the effect of road geometry error on the *performance of tracking and behavior reasoning*, the state estimate errors for the distance, heading and speed of the tracking results (Fig. 26) and the number of misclassification to the incorrect behaviors (Fig. 27) are analyzed respectively. From the results of state estimate errors of Fig. 26, we can figure out that the tracking performance is stable under the 0.45 meters of the roadway geometry map error. However, it is difficult to estimate the trend of the tracking error if the roadways map error is over than 0.45 meters. From the results of behavior reasoning for Fig. 27, we can expect that the behavior reasoning is reliable under the 0.25 meters of the roadway error. However, if the roadways map error is larger than 0.25 meters, the behavior reasoning algorithm starts to misclassify the target vehicle's behavior. From these two analysis results for the tracking and behavior reasoning, we can conclude that the maximum error boundary of the roadway geometry map is about 0.25 meters.

VII. Conclusion

The paper proposed a unified motion tracking and behavior reasoning algorithm for moving vehicles located near the ego vehicle. The results of this study can be summarized as follows.

1) Roadway geometry constraints were utilized in the vehicle motion tracking and behavior reasoning algorithm. The roadway geometry information can be obtained from the digital map referencing the ego vehicle location data from the localization system. The roadway geometry information was used to construct the curvilinear coordinate system. The proposed unified tracking and behavior

reasoning was performed based on the curvilinear coordinate system. The curvilinear coordinate system makes the design problem of vehicle tracking filter more intuitive by proposing guidelines to tune the covariance matrix of the filter. Furthermore, conversion to the curvilinear coordinate system can improve the performance of the driving behavior classification by describing the vehicle motion along the roadway geometry.

2) Multiple model sets were designed to represent various vehicle motions and behaviors based on the curvilinear coordinate system. The multiple model sets consisted of four types of motion: constant velocity lane keeping (CVLK), constant acceleration lane keeping (CALK), constant velocity lane changing (CVLC), and constant acceleration lane changing (CALC). Since the models are designed in curvilinear coordinates, it is possible to design the vehicle motion model using linear equations. Therefore, it is possible to apply standard Kalman filter that is more computationally efficient than various nonlinear filters such as an extended Kalman filter, unscented Kalman filter, and particle filter in the tracking algorithm.
3) The paper presents unified frameworks to simultaneously track the vehicle motion and infer the behavior of vehicles. The IMM filter was used as a basis of unified tracking and behavior reasoning because the IMM filter can simultaneously infer the vehicle behavior by finding the appropriate behavior model based on the model probabilities and estimate the vehicle motion by weighing the filtering result of the selected behavior model.
4) The experimental results show that the heading accuracy improved compared to the tracking algorithm within the Cartesian coordinate system. However, there are no many improvements for the position estimate due to the non-Gaussian noise from the bounding box association error of the LIDARs. This accuracy improvement can enhance the performance of the vehicle motion prediction for the motion planning system. Furthermore, the behavior reasoning results can also be used to improve the motion and behavior prediction.

However, the proposed algorithm does not cope with situations at linked roadway areas such as merges, splits, and intersections because the problems are related to the roadway routing problems which can make the problem more difficult. In addition, the proposed four behaviors used for the behavior reasoning cannot cover the abnormal driving situation such as traffic accidents and a driving on the construction sites. In future work, the authors plan to extend the algorithm in order to cover the linked roadway areas and the behaviors for the abnormal conditions.

APPENDIX

One cycle of the IMM filter for n models can be described by the following equations.

1) Interacting (for model index $i = 1, 2, \ldots, n$):
   - Predicted model probability:
$$\hat{\mu}_{k|k-1}^{(i)} = P\left\{m_k^{(i)}|z^{k-1}\right\} = \sum_j \pi_{ji}\mu_{k-1}^{(j)}.$$
   - Mixing weight:
$$\mu_{k-1}^{j|i} = P\left\{m_{k-1}^{(j)}|m_k^{(i)}, z^{k-1}\right\} = \pi_{ji}\mu_{k-1}^{(j)} \Big/ \hat{\mu}_{k|k-1}^{(i)}.$$
   - Mixing estimate:
$$\bar{x}_{k-1|k-1}^{(i)} = E\left\{x_{k-1}|m_k^{(i)}, z^{k-1}\right\} = \sum_j \hat{x}_{k-1|k-1}^{(j)}\mu_{k-1}^{j|i}.$$
   - Mixing covariance:
$$\hat{P}_{k-1|k-1}^{(i)} = \sum_j \left[P_{k-1|k-1}^{(j)} + \left(\bar{x}_{k-1|k-1}^{(i)} - \hat{x}_{k-1|k-1}^{(j)}\right) \times \left(\bar{x}_{k-1|k-1}^{(i)} - \hat{x}_{k-1|k-1}^{(j)}\right)^T\right]\mu_{k-1}^{j|i}.$$
2) Elementary filters:
   - Predicted state:
$$\hat{x}_{k|k-1}^{(i)} = F_{k-1}^{(i)}\bar{x}_{k-1|k-1}^{(i)} + G_{k-1}^{(i)}u_{k-1}^{(i)} + \bar{w}_{k-1}^{(i)}.$$
   - Predicted covariance:
$$P_{k|k-1}^{(i)} = F_{k-1}^{(i)}\bar{P}_{k-1|k-1}^{(i)}\left(F_{k-1}^{(i)}\right)^T + L_{k-1}^{(i)}Q_{k-1}^{(i)}\left(L_{k-1}^{(i)}\right)^T.$$
   - Measurement residual:
$$\tilde{z}_k^{(i)} = z_k - H_k^{(i)}\hat{x}_{k-1|k-1}^{(i)} - \bar{v}_k^{(i)}.$$
   - Residual covariance:
$$S^{(i)} = H_k^{(i)}P_{k|k-1}^{(i)}\left(H_k^{(i)}\right)^T + R_k^{(i)}.$$
   - If the measurement is inside the validation gate:
$$\tilde{V}_{g^2}(k) = (\tilde{z}_k)^T(S_k)^{-1}\tilde{z}_k \le g^2.$$
   - — Filter gain: $K_k^{(i)} = P_{k|k-1}^{(i)}(H_k^{(i)})^T(S_k^{(i)})^{-1}$
   - — Updated state: $\hat{x}_{k|k}^{(i)} = \hat{x}_{k|k-1}^{(i)} + K_k^{(i)}\tilde{z}_k^{(i)}$
   - — Updated covariance: $P_{k|k}^{(i)} = P_{k|k-1}^{(i)} - K_k^{(i)}S_k^{(i)}(K_k^{(i)})^T$
3) Model probability update:
   - Model likelihood:
$$L_k^{(i)} = p\left[\tilde{z}_k^{(i)}|m_k^{(i)}, z^{k-1}\right] = \frac{\exp\left[-\frac{1}{2}\left(\tilde{z}_k^{(i)}\right)^T\left(S_k^{(i)}\right)^{-1}\tilde{z}_k^{(i)}\right]}{\sqrt{(2\pi)^{\dim(z)}\left|S_k^{(i)}\right|}}.$$
   - Model probability:
$$\mu_k^{(i)} = P\left\{m_k^{(j)}|z^k\right\} = \frac{\hat{\mu}_{k|k-1}^{(i)}L_k^{(i)}}{\sum_j \hat{\mu}_{k|k-1}^{(j)}L_k^{(j)}}.$$

4) Combination:
   - Overall estimate: $\hat{x}_{k|k} = E[x_k|z^k] = \sum_i \hat{x}^{(i)}_{k|k-1}\mu^{(i)}_k$
   - Overall covariance:

$$P_{k|k} = \sum_i \left[P^{(i)}_{k|k} + \left(\hat{x}_{k|k} - \hat{x}^{(i)}_{k|k}\right)\left(\hat{x}_{k|k} - \hat{x}^{(i)}_{k|k}\right)^T \right] \mu^{(i)}_k.$$

ACKNOWLEDGMENT

The authors would like to thank their team members of the smart car research group (SRG) of the *ACE Lab* for helpful discussions and for their great contribution to develop the autonomous car *A1*.

REFERENCES

[1] C. Hoffmann, T. Dang, and C. Stiller, "Vehicle detection fusing 2D visual features," in *Proc. IEEE Intell. Veh. Symp.*, 2004, pp. 280–285.
[2] A. Jazayeri, H. Cai, J. Y. Zheng, and M. Tuceryan, "Vehicle detection and tracking in car video based on motion model," *IEEE Trans. Intell. Transp. Syst.*, vol. 12, no. 2, pp. 583–595, Jun. 2011.
[3] A. Broggi, P. Cerri, and P. C. Antonello, "Multi-resolution vehicle detection using artificial vision," in *Proc. IEEE Intell. Veh. Symp.*, 2004, pp. 310–314.
[4] S. Gupte, O. Masoud, R. F. K. Martin, and N. P. Papanikolopoulos, "Detection and classification of vehicles," *IEEE Trans. Intell. Transp. Syst.*, vol. 3, no. 1, pp. 37–47, Mar. 2002.
[5] I. Sato, C. Yamano, and H. Yanagawa, "Crossing obstacle detection with a vehicle-mounted camera," in *Proc. IV*, 2011, pp. 60–65.
[6] F. Erbs, A. Barth, and U. Franke, "Moving vehicle detection by optimal segmentation of the dynamic stixel world," in *Proc. IEEE IV*, 2011, pp. 951–956.
[7] F. Nashashibi and A. Bargeton, "Laser-based vehicles tracking and classification using occlusion reasoning and confidence estimation," in *Proc. IEEE Intell. Veh. Symp.*, 2008, pp. 847–852.
[8] F. Fayad and V. Cherfaoui, "Tracking objects using a laser scanner in driving situation based on modeling target shape," in *Proc. IEEE Intell. Veh. Symp.*, 2007, pp. 44–49.
[9] A. Ewald and V. Willhoeft, "Laser scanners for obstacle detection in automotive applications," in *Proc. IEEE Intell. Veh. Symp.*, 2000, pp. 682–687.
[10] J. Gunnarsson, L. Svensson, L. Danielsson, and F. Bengtsson, "Tracking vehicles using radar detections," in *Proc. IEEE Intell. Veh. Symp.*, 2007, pp. 296–302.
[11] R. Möbus and U. Kolbe, "Multi-target multi-object tracking, sensor fusion of radar and infrared," in *Proc. IEEE Intell. Veh. Symp.*, 2004, pp. 732–737.
[12] M. Heuer, A. Al-Hamadi, A. Rain, and M. M. Meinecke, "Detection and tracking approach using an automotive radar to increase active pedestrian safety," in *Proc. IEEE Intell. Veh. Symp.*, 2014, pp. 890–893.
[13] F. Fölster and H. Rohling, "Data association and tracking for automotive radar networks," *IEEE Trans. Intell. Transp. Syst.*, vol. 6, no. 1, pp. 370–377, Dec. 2005.
[14] H. Weigel, P. Lindner, and G. Wanielik, "Vehicle tracking with lane assignment by camera and Lidar sensor fusion," in *Proc. IEEE Intell. Veh. Symp.*, 2009, pp. 513–520.
[15] M. S. Darms, P. E. Rybski, C. Baker, and C. Urmson, "Obstacle detection and tracking for the urban challenge," *IEEE Trans. Intell. Transp. Syst.*, vol. 10, no. 3, pp. 475–485, Sep. 2009.
[16] Q. Baig, O. Aycard, T. D. Vu, and T. Fraichard, "Fusion between laser and stereo vision data for moving objects tracking in intersection like scenario," in *Proc. IEEE IV*, 2011, pp. 362–367.
[17] C. Hyunggi, S. Young-Woo, B. V. K. Vijaya Kumar, and R. R. Rajkumar, "A multi-sensor fusion system for moving object detection and tracking in urban driving environments," in *Proc. IEEE ICRA*, 2014, pp. 1836–1843.
[18] S. Matzka and R. Altendorfer, "A comparison of track-to-track fusion algorithms for automotive sensor fusion," in *Proc. IEEE Int. Conf. MFI Intell. Syst.*, 2008, pp. 189–194.
[19] M. Ardelt, C. Coester, and N. Kaempchen, "Highly automated driving on freeways in real traffic using a probabilistic framework," *IEEE Trans. Intell. Transp. Syst.*, vol. 13, no. 4, pp. 1576–1585, Dec. 2012.
[20] Y. Hou, P. Edara, and C. Sun, "Situation assessment and decision making for lane change assistance using ensemble learning methods," *Expert Syst. Appl.*, vol. 42, pp. 3875–3882, 2015.
[21] Y. Hou, P. Edara, and C. Sun, "Modeling mandatory lane changing using bayes classifier and decision trees," *IEEE Trans. Intell. Transp. Syst.*, vol. 15, no. 2, pp. 647–655, Apr. 2014.
[22] J. E. Naranjo, C. Gonzalez, R. Garcia, and T. de Pedro, "Lane-change fuzzy control in autonomous vehicles for the overtaking maneuver," *IEEE Trans. Intell. Transp. Syst.*, vol. 9, no. 3, pp. 438–450, Sep. 2008.
[23] R. Dang, J. Wang, S. E. Li, and K. Li, "Coordinated adaptive cruise control system with lane-change assistance," *IEEE Trans. Intell. Transp. Syst.*, vol. 16, no. 5, pp. 2373–2383, Oct. 2015.
[24] X. Guoqing, L. Li, O. Yongsheng, and S. Zhangjun, "Dynamic modeling of driver control strategy of lane-change behavior and trajectory planning for collision prediction," *IEEE Trans. Intell. Transp. Syst.*, vol. 13, no. 3, pp. 1138–1155, Sep. 2012.
[25] S. Ammoun, F. Nashashibi, and C. Laurgeau, "An analysis of the lane changing manoeuvre on roads: The contribution of inter-vehicle cooperation via communication," in *Proc. IEEE IV*, Istanbul, Turkey, 2007, pp. 1095–1100.
[26] J. Qiu, W. Guoyuan, K. Boriboonsomsin, and M. Barth, "Improving traffic operations using real-time optimal lane selection with connected vehicle technology," in *Proc. IEEE Intell. Veh. Symp.*, 2014, pp. 70–75.
[27] S. Sivaraman and M. M. Trivedi, "Dynamic probabilistic drivability maps for lane change and merge driver assistance," *IEEE Trans. Intell. Transp. Syst.*, vol. 15, no. 5, pp. 2063–2073, Oct. 2014.
[28] M. Althoff, O. Stursberg, and M. Buss, "Model-based probabilistic collision detection in autonomous driving," *IEEE Trans. Intell. Transp. Syst.*, vol. 10, no. 2, pp. 299–310, Jun. 2009.
[29] M. Althoff, O. Stursberg, and M. Buss, "Safety assessment of driving behavior in multi-lane traffic for autonomous vehicles," in *Proc. IEEE Intell. Veh. Symp.*, Xi'an, China, 2009, pp. 893–900.
[30] R. Schubert and G. Wanielik, "A unified Bayesian approach for object and situation assessment," *IEEE Intell. Transp. Syst. Mag.*, vol. 3, no. 2, pp. 6–19, Summer 2011.
[31] D. Kasper *et al.*, "Object-oriented Bayesian networks for detection of lane change maneuvers," *IEEE Intell. Transp. Syst. Mag.*, vol. 4, no. 3, pp. 19–31, Fall 2012.
[32] J. Kim, K. Jo, W. Lim, M. Lee, and M. Sunwoo, "Curvilinear-coordinate-based object and situation assessment for highly automated vehicles," *IEEE Trans. Intell. Transp. Syst.*, vol. 16, no. 3, pp. 1–17, Jun. 2015.
[33] J. Kichun, C. Keonyup, and S. Myoungho, "GPS-bias correction for precise localization of autonomous vehicles," in *Proc. IEEE IV*, 2013, pp. 636–641.
[34] K. Jo, K. Chu, and M. Sunwoo, "Interacting multiple model filter-based sensor fusion of GPS with in-vehicle sensors for real-time vehicle positioning," *IEEE Trans. Intell. Transp. Syst.*, vol. 13, no. 1, pp. 329–343, Mar. 2012.
[35] K. Jo and M. Sunwoo, "Generation of a precise roadway map for autonomous cars," *IEEE Trans. Intell. Transp. Syst.*, vol. 15, no. 3, pp. 925–937, Jun. 2014.
[36] S. Matzka and R. Altendorfer, "A comparison of track-to-track fusion algorithms for automotive sensor fusion," in *Multisensor Fusion and Integration for Intelligent Systems*. New York, NY, USA: Springer-Verlag, 2009, pp. 69–81.
[37] M. Aeberhard, A. Rauch, M. Rabiega, N. Kaempchen, and T. Bertram, "Track-to-track fusion with asynchronous sensors and out-of-sequence tracks using information matrix fusion for advanced driver assistance systems," in *Proc. IEEE IV*, 2012, pp. 1–6.
[38] I. Skog and P. Handel, "Time synchronization errors in loosely coupled GPS-aided inertial navigation systems," *IEEE Trans. Intell. Transp. Syst.*, vol. 12, no. 4, pp. 1014–1023, Dec. 2011.
[39] T. Huck, A. Westenberger, M. Fritzsche, T. Schwarz, and K. Dietmayer, "Precise timestamping and temporal synchronization in multi-sensor fusion," in *Proc. IEEE IV*, 2011, pp. 242–247.
[40] H. Wang, J. Kearney, and K. Atkinson, "Robust and efficient computation of the closest point on a spline curve," in *Proc. 5th Int. Conf. Curves Surfaces*, 2002, pp. 397–406.
[41] M. Tomizuka, S. Patwardhan, and Z. Wei-Bin, "Experimental study of lane change manoeuvre for AHS applications," in *Proc. Amer. Control Conf.*, 1995, vol. 1, pp. 139–143.
[42] C. Hatipoglu, U. Ozguner, and K. A. Redmill, "Automated lane change controller design," *IEEE Trans. Intell. Transp. Syst.*, vol. 4, no. 1, pp. 13–22, Mar. 2003.
[43] H. A. P. Blom and Y. Bar-Shalom, "Interacting multiple model algorithm for systems with Markovian switching coefficients," *IEEE Trans. Autom. Control*, vol. 33, no. 1, pp. 780–783, Jan. 1988.
[44] S. Lefèvre, D. Vasquez, and C. Laugier, "A survey on motion prediction and risk assessment for intelligent vehicles," *Robomech J.*, vol. 1, p. 1, 2014.

Kichun Jo (S'10–M'14) received the B.S. degree in mechanical engineering and the Ph.D. degree in automotive engineering from Hanyang University, Seoul, South Korea, in 2008 and 2014, respectively.

Between 2014 and 2015, he was with the Automotive Control and Electronics Laboratory (ACE Lab), Department of Automotive Engineering, Hanyang University, doing research on system design and implementation of autonomous cars. Since 2015, he has been with Valeo, Paris, France, working on the highly automated driving. His main interests include localization and mapping, objects tracking, information fusion, vehicle state estimation, behavior planning, and vehicle motion control for highly automated vehicles. His current research activities include hardware and software platform design of autonomous cars based on distributed real-time embedded systems and in-vehicle networks.

Minchul Lee (S'14) received the B.S. degree in mechanical engineering from Hanyang University, Seoul, South Korea, in 2013, where he is currently working toward the Ph.D. degree in the Automotive Control and Electronics Laboratory.

His main interests include precise positioning and localization, vehicle motion assessment, information fusion theories, real-time systems for autonomous cars, and the system of autonomous vehicles. His current research activities include vehicle motion assessment for autonomous cars.

Junsoo Kim (S'11–M'15) received B.S. degree in mechanical engineering and the Ph.D. degree in automotive engineering from Hanyang University, Seoul, South Korea, in 2008 and 2015, respectively.

Since 2015, he has been with ADAS Strategy Team, Hyundai Motor Company Korea, Seoul, focusing on the autonomous driving system. His main interests include vehicle control, decision theories, motion planning algorithms, and real-time systems. His current research activities include behavior reasoning and trajectory planning of highly automated vehicles. He has also worked on model-based embedded software development for automotive control systems.

Myoungho Sunwoo (M'81) received the B.S. degree in electrical engineering from Hanyang University, Seoul, South Korea, in 1979, the M.S. degree in electrical engineering from the University of Texas at Austin, Austin, TX, USA, in 1983, and the Ph.D. degree in system engineering from Oakland University, Rochester, MI, USA, in 1990.

He joined General Motors Research (GMR) Laboratories, Warren, MI, USA, in 1985 and has worked in the area of automotive electronics and control for 30 years. During his nine-year tenure with GMR, he worked on the design and development of various electronic control systems for power trains and chassis. Since 1993, he has led research activities as a Professor with the Department of Automotive Engineering, Hanyang University. His work has focused on automotive electronics and controls such as modeling and control of internal combustion engines, design of automotive distributed real-time control systems, intelligent autonomous vehicles, and automotive education programs.